GEOPHYSICS, VOL. 76, NO. 1 (JANUARY-FEBRUARY 2011); P. T1–T11, 14 FIGS.
10.1190/1.3511524

Converted waves in a shallow marine environment: Experimental and modeling studies

Nihed Allouche[1], Guy G. Drijkoningen[1], Willem Versteeg[2], and Ranajit Ghose[1]

ABSTRACT

Seismic waves converted from compressional to shear mode in the shallow subsurface can be useful not only for obtaining shear-wave velocity information but also for improved processing of deeper reflection data. These waves generated at deep seas have been used successfully in hydrocarbon exploration; however, acquisition of good-quality converted-wave data in shallow marine environments remains challenging. We have looked into this problem through field experiments and synthetic modeling. A high-resolution seismic survey was conducted in a shallow-water canal using different types of seismic sources; data were recorded with a four-component water-bottom cable. Observed events in the field data were validated through modeling studies. Compressional waves converted to shear waves at the water bottom and at shallow reflectors were identified. The shear waves showed distinct linear polarization in the horizontal plane and low velocities in the marine sediments. Modeling results indicated the presence of a nongeometric shear-wave arrival excited only when the dominant wavelength exceeded the height of the source with respect to the water/sediment interface, as observed in air-gun data. This type of shear wave has a traveltime that corresponds to the raypath originating not at the source but at the interface directly below the source. Thus, these shear waves, excited by the source/water-bottom coupled system, kinematically behave as if they were generated by an S-wave source placed at the water bottom. In a shallow-water environment, the condition appears to be favorable for exciting such shear waves with nongeometric arrivals. These waves can provide useful information of shear-wave velocity in the sediments.

INTRODUCTION

Shear-wave velocity V_S provides important information for characterizing the shallow marine subsurface. We note that V_S differs from P-wave velocity V_P because of the sensitivity of V_S to pore content and hence strong correlation with lithology variations (Gregory, 1976; Hamilton, 1976). From in situ and core measurements of the upper tens of meters of marine sediments, many authors (e.g., Theilen and Pecher, 1991; Ewing et al., 1992; Ayres and Theilen, 1999) report that V_S increases rapidly with depth, whereas V_P remains nearly constant. The availability of P- and S-wave information allows one to estimate lithological properties such as porosity and grain size through empirical relations (Domenico, 1984).

Geotechnical studies also benefit from retrieving V_S in marine sediments. This is because physical properties such as shear strength can be correlated to V_S and used for estimating seafloor stability and assessing geohazards, in addition to many other engineering purposes (Kugler et al., 2007). Furthermore, obtaining accurate V_S models of the shallow subsurface is advantageous for the processing of multicomponent seismic data (e.g., wavefield decomposition, static correction) and imaging targets below shallow gas pockets (Granli et al., 1999).

Various seismic methods can be used to infer V_S models of shallow marine sediments. These methods differ primarily in the type of waves acquired. In 1984, Kiel University developed a seabed air-gun source capable of generating horizontal shear stress (Gehrmann et al., 1984). This source was used for refraction surveys and enabled the recording of SH-waves using horizontal geophones. A similar shear-wave source with dual air-gun drive has been presented by Chmela (2003). This air-gun shear-wave source generates a large amount of P- and P-SV-wave energy and a considerably limited amount of SH-wave energy. More recently, the Norwegian Geotechnical Institute has developed a sea-bed coupled vibratory source that appears to generate pure SH-waves (Westerdahl et al., 2004). This

Manuscript received by the Editor 7 September 2009; revised manuscript received 31 March 2010; published online 5 January 2011.
[1]Delft University of Technology, Department of Geotechnology, Delft, The Netherlands. E-mail: n.elallouche@tudelft.nl; g.g.drijkoningen@tudelft.nl; r.ghose@tudelft.nl.
[2]Ghent University, Department of Geology and Soil Science, Ghent, Belgium. E-mail: willem.versteeg@ugent.be.

electrohydraulic marine vibrator weighs 9 tons, and the source frequency band is restricted to 2–45 Hz. Seabed coupled shear-wave sources have not yet seen wide application because they do not allow fast acquisition: source and receiver are placed at the water bottom.

To estimate the seismic properties of shallow marine sediments, Riedel and Theilen (2001) invert the AVO signature of P-waves. They obtain good results for the P-wave velocity and density but conclude that the S-wave velocity is difficult to estimate. The uncertainties in the derived V_S values are attributed to the insensitivity of the P-wave reflection amplitude to the estimated parameter in the environment of interest.

Another popular approach is to invert the dispersion curves of the Scholte wave (e.g., Caiti et al., 1994; Ritzwoller and Levshin, 2002; Park et al., 2005). These P-SV polarized waves, traveling along the water-bottom interface, are highly sensitive to the shear-wave velocity. The Scholte waves are generated by an air-gun source and are recorded using a receiver array placed in the water or at the water bottom. The recorded modes are resolved and inverted to obtain V_S profiles.

Shear-wave velocity can also be determined from converted waves, i.e., waves converted from compressional to shear mode at the water bottom or at a subsurface reflector. In hydrocarbon exploration, these waves have been used successfully for many years (e.g., Stewart et al., 2003). Our research has focused on this mode of shear-wave generation, but for shallow marine environments. Modeling studies show that the conversion of incident plane waves at the water bottom is very small and that waves converted once at a shallow reflector and recorded in the horizontal component are most likely to be observed only at large offsets (Allouche et al., 2008).

In the present study, we investigate whether converted waves are observable in field data in a shallow marine environment. We present the results of a multicomponent seismic survey conducted by deploying a four-component (4C) receiver array in a shallow-water canal. The results of field data analyses and new modeling studies are then discussed to establish the presence of two types of converted shear waves in such a shallow-water environment. Further, we present, for the first time, evidence of nongeometric events in the shallow marine data, which we interpret as shear waves. Finally, the excitation criteria for such waves at the proximity of the water/sediment interface are discussed.

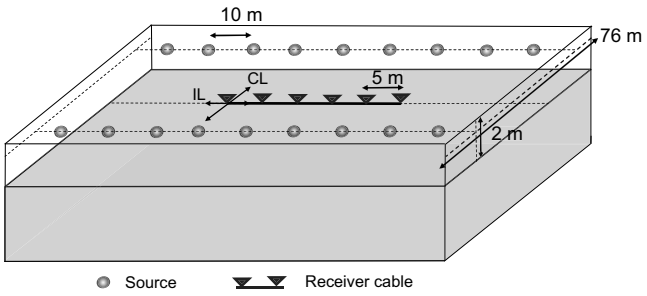

Figure 1. Sketch of the field setting in the survey area. The arrows at the receiver denote the direction of the inline (IL) and crossline (CL) components.

FIELD EXPERIMENT

A high-resolution seismic survey was conducted in 2004 in a shallow-water canal near Ghent, Belgium. Two seismic lines were shot using various types of sources, including an air gun, a water gun, and a sparker. The source was towed at a water depth of 1 m and fired at a spacing of 10 m. The data were acquired using a 4C water-bottom cable spread at a water depth of 2 m. The cable consisted of 12 receivers at 5-m spacing. A schematic of the field configuration is given in Figure 1. The air-gun data were sampled at 0.25 ms and recorded for 2 s.

Because of the limited number of receivers, the processing and analysis of the multicomponent air-gun data were performed in the common-receiver domain. For each component, 12 receivers contained 107 traces each. The data redundancy and quality can be improved if we assume that the subsurface below the cable is laterally invariant — an assumption quite acceptable for this well-known area. By sorting every two adjacent receiver gathers according to offset and then merging them, we obtained six new gathers, each with a double number of sources and half the original shot spacing. To increase the signal-to-noise ratio (S/N), the obtained receiver gathers were normalized per trace and summed together, finally resulting in one gather. A band-pass filter of 12–120 Hz was subsequently applied to the data. Figure 2 shows the enhancement of event

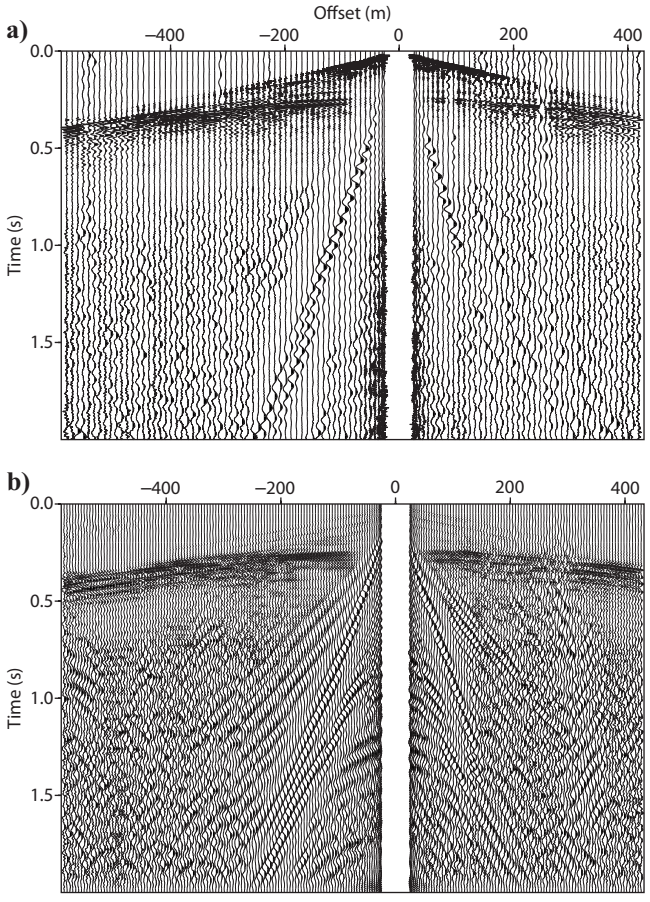

Figure 2. Common-receiver gather acquired using an air gun and recorded on the hydrophone component. (a) Raw data and (b) processed data after applying automatic gain control (AGC) with a time window of 0.4 s.

coherency achieved for the hydrophone component after applying the processing steps.

MULTICOMPONENT ANALYSIS

Although the absence of sonic logs and multicomponent VSP data prevent conclusive interpretations, the nature of the seismic events can still be revealed based on their fundamental differences. Because S-waves are polarized in the direction perpendicular to the propagation, they are expected to be dominant at a different component than the P-waves. Depending on their raypath, S-waves have a relatively strong amplitude in data recorded on the horizontal components, whereas P-waves are mainly observed on the vertical component. As a result of the low velocity, S-waves appear at later times than the P-waves; they have a low moveout velocity. Specifically for shallow unconsolidated sediments encountered in the study area, the V_P/V_S ratio was expected to be very high and to have a drastic effect on the moveout velocity of the converted waves. In this analysis, we used the particle motion and the difference in moveout velocity as attributes to identify the recorded seismic events.

The processed common-receiver gathers corresponding to each component are shown in Figure 3. A few distinctive features consistently observed in the data are marked in these gathers. The high-frequency early arrivals, present in all components but significantly strong on the pressure measurement (hydrophone), are P-wave reflections. The dispersive events, also dominant in all components, are interface waves traveling along the water/sediment boundary. In addition to these arrivals, three other types of events draw our attention. These are highlighted by outlines of three different colors in Figure 3 and are analyzed in the following paragraphs, taking into account their particle motion and moveout velocity.

Particle motion

The polarization direction is indicative of the type of event involved; therefore, it is often used as a tool for event discrimination. Before computing the particle motion of the selected events in the data, we had to correct for the crossline offset between the shot line and the receiver array. Knowing the orientation of the geophone cable from the field geometry (Figure 1), we rotated the horizontal components through a given angle for each shot point so that the new axes lay along the radial and transverse directions.

Figure 4 shows an enlarged part of the rotated components and the pressure component containing the distinctive arrivals with their particle motion. These arrivals are highlighted with the same colors as their corresponding outlines in Figure 3. Evaluation of the particle

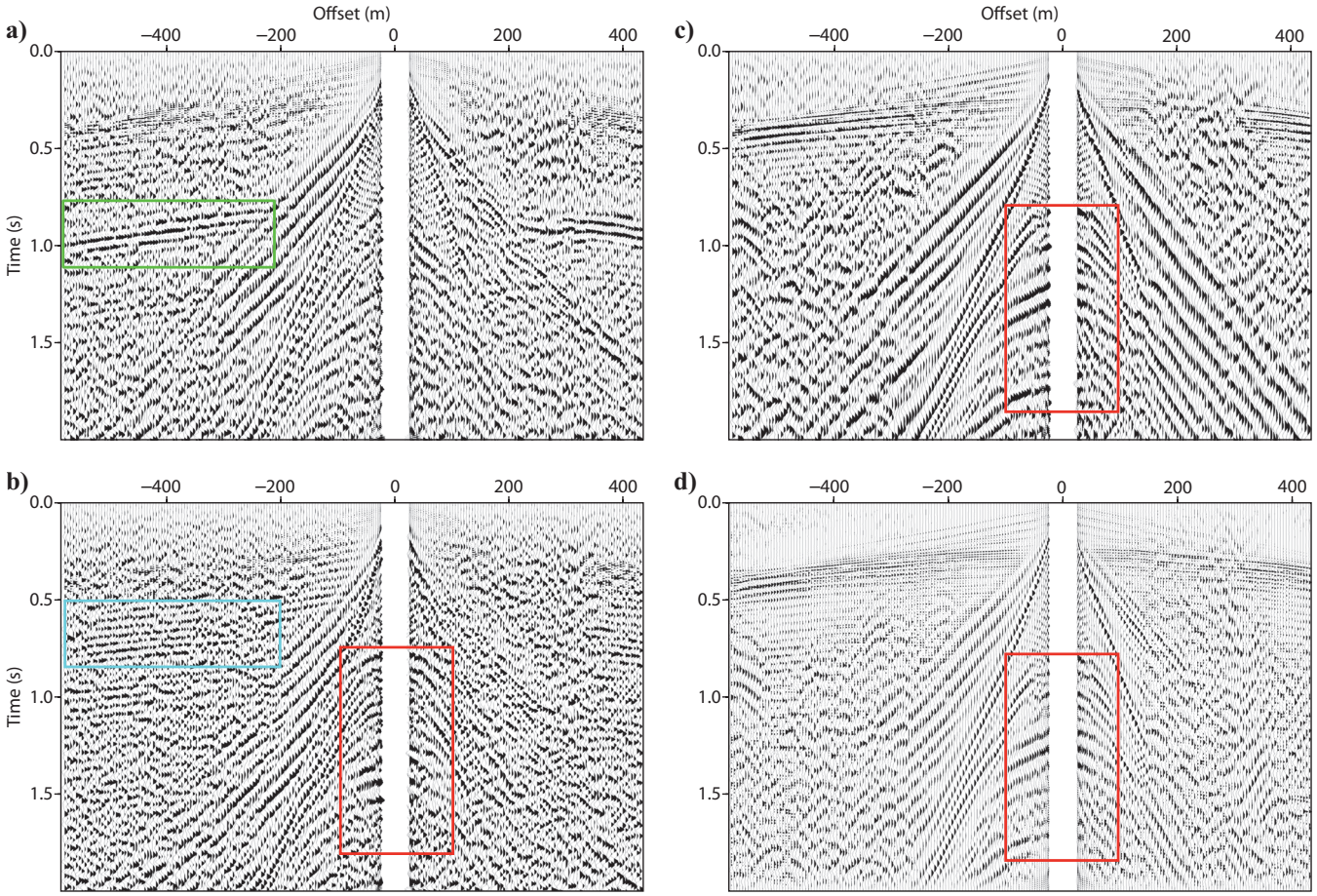

Figure 3. Common-receiver gathers recorded on (a) inline, (b) crossline, (c) vertical, and (d) hydrophone components. Outlines in three different colors highlight the distinctive events.

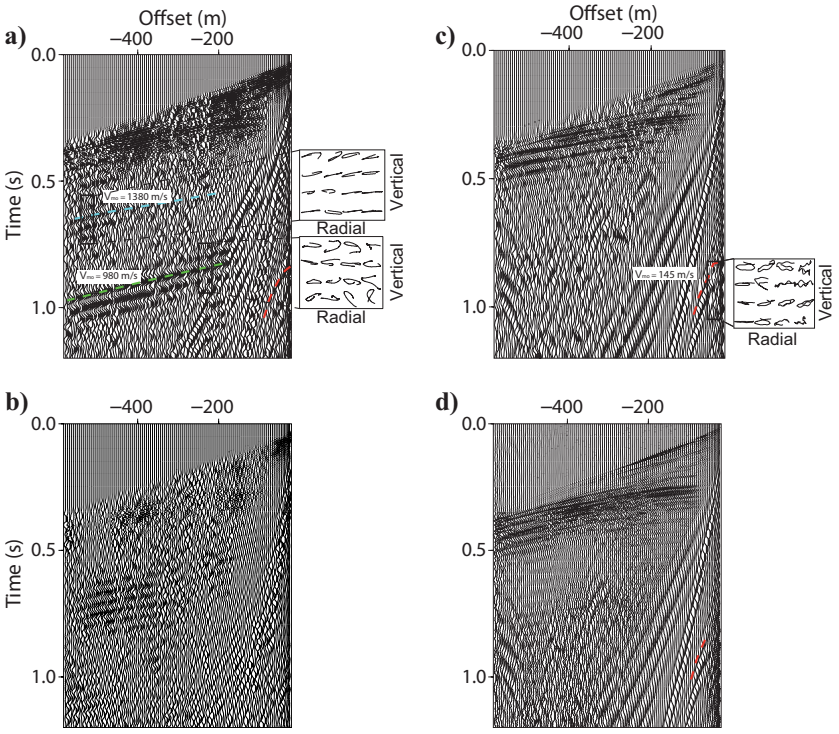

Figure 4. Common-receiver gathers after rotation: (a) radial, (b) transverse, (c) vertical, and (d) pressure components. The moveout velocity and the particle motion of the marked events are included. The black frames indicate the size of the window used to compute the particle motion.

motion using the radial and vertical components shows that all of the highlighted events are polarized in the horizontal plane. We also notice that the events enclosed in the blue outline in Figure 3 still have energy present in the transverse component after the rotation.

Moveout velocity

In situ measurement of shallow marine sediments shows that V_P/V_S ratios can be very high in the upper few tens of meters. The values can range from six for water-saturated sands to 13 or even higher for silty clays (Hamilton, 1979). This is expected to have a strong effect on the appearance of the converted events in the data.

In Figure 4, we indicate the moveout velocities of the highlighted events. The hyperbolic event with the red dashed line has a moveout velocity of 145 m/s (Figure 4c). This value is unrealistically low for a wave converting geometrically from P to S at any interface, which suggests that this event has traveled solely as a shear wave in the sediment. The event marked by the blue dashed line has a velocity of 1380 m/s and a relatively small delay in time compared to the P-waves (Figure 4a). The implication is that the mode has traveled mainly as a P-wave before converting at a reflector to an S-wave. The last reflection shown by the green dashed line arrives later and has a lower moveout velocity (Figure 4a), which may indicate that they have traveled an important part of their path as an S-wave. Therefore, this arrival can be interpreted as a P-wave converted at the water bottom to an S-mode. It is also possible that this arrival includes other refracted events that may coincide with the interpreted converted wave at small range.

MODELING STUDY

To better understand the nature of the distinctive events observed in the field data and to investigate whether shear waves have been excited directly by an air gun, we conducted a modeling study. We

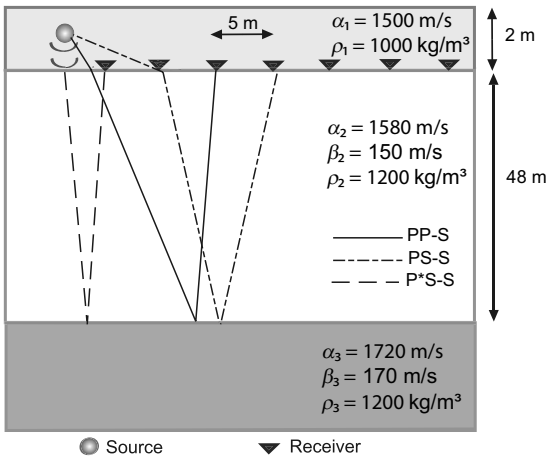

Figure 5. Sketch of the model used to generate the synthetic data. The travelpaths of the converted modes (PP-S, PS-S, and P*S-S) are depicted. The shading below the source denotes the nongeometric path of the P-wave in the water for the converted P*S-S-mode.

chose a simple three-layer model to avoid unnecessary complicated responses that might obstruct our understanding. The model consisted of a water layer overlying two sediment layers with P-wave velocities ranging from 1580 to 1720 m/s (Figure 5). The thickness of the layers and the velocity values were obtained from a velocity analysis performed on the hydrophone component of the field data. Furthermore, we assumed a change of density from 1000 kg/m^3 in the water to 1200 kg/m^3 in the sediments. We did not have any constraints on the S-wave velocity, so we assumed a V_P/V_S of 10, which is realistic for the shallow, unconsolidated sediments encountered in the survey area. The dominant frequency of the source wavelet was 80 Hz, as estimated from the direct wave in the field data. The acqui-

sition parameters in our modeling were kept similar to the field experiment. To compute the seismic response, we used a semianalytical algorithm developed to solve the homogeneous wave equation for horizontally stratified media (Schmidt and Tango, 1986); the software package is known as Oases (Schmidt, 1988).

Our modeled response is compared with the field data in Figure 6. We note some distinct similarities. For example, the synthetic data show that the reflection marked with the blue dashed line is a P-wave converted to an S-wave at a reflector (PP-S), whereas the reflection indicated by the green dashed line is converted at the water bottom (PS-S) (Figure 6). The PP-S arrival is the mode of conversion typically used at the exploration scale. Note that the PP-S-mode has the same traveltime as the PS-P-mode but only in the case of horizontally layered media. At small offsets, the arrival identified as PS-S is interfering with two other refracted modes. The travelpaths and traveltime of these refracted waves are discussed in Appendix A.

Moreover, the low-frequency hyperbolic event arriving at 0.65 s can be correlated with the reflection marked by the red dashed line in the field data in Figures 4 and 6. This event is asymptotic to the Scholte wave and has the traveltime of an S-wave reflection as if it has been generated at the water bottom. The longer traveltime of this reflection in the field data suggests in reality a lower average S-wave velocity than the assumed 150 m/s in the shallowest marine sediments. As explained in Appendix A, the observed reflection clearly has a different moveout than what is expected for the S-wave converted at the water bottom according to Snell's law. The excitation of this nongeometric shear-wave reflection (P^*S-S, where the asterisk denotes the nongeometric travelpath in water) is source coupled because it was not observed in the water-gun data or in the sparker data. At near offsets, the P^*S-S reflection has the same traveltime as the PS-S arrival. As offset increases, the moveout of the nongeometric shear-wave reflection diverges from that of the PS-S-wave. The excitation of this particular shear wave is discussed in the following section.

Another peculiar observation is the presence of these slow nongeometric waves in the pressure component of the field and synthetic data. This shows that these shear waves are converted to P-modes at the water-bottom interface. In contrast with the other converted modes (PS-S, PP-S, and PS-P), this S-P conversion is significant because these waves are well visible in the hydrophone recording (see Figure 6e and f).

EXCITATION OF SHEAR WAVES BY SOURCE/WATER-BOTTOM COUPLED SYSTEM

The low-frequency reflected events propagating with an S-wave velocity were only visible in the air-gun data. In Figure 7, a common-receiver gather acquired using an air gun is compared with one generated by a water gun. The two sources differ primarily in frequency content, with the air gun having a lower dominant frequency. The field configuration was kept the same during the survey, so the excitation of the nongeometric shear wave seem to be related to near-field effects.

To understand this excitation, it is sufficient to consider the transmission across a fluid/solid contact with the same seismic properties as the studied area. The interaction of the incident fluid wave with the water-bottom interface is determined by the ratio between the source height h and the dominant wavelength λ. A large ratio h/λ implies a far-field condition. The incident wave can then be assumed to be planar and the energy partitioning to be governed by the Zoeppritz equations. However, the situation becomes different when the ratio is low; it can be fractional if the wavelength exceeds the height of the source from the water/sediment interface. The incident spherical wave will then interact with the water bottom and give rise to shear waves, Scholte waves, and head waves. The snapshot images (cross sections) of particle velocity, computed for both situations using a finite-difference algorithm, are illustrated in Figure 8. The horizontal particle velocity computed for receivers at depth is also shown in Figure 8. The nongeometric PS-wave is observed only in the near-field case; it is the arrival diverging from the geometric PS-wave at a certain offset.

The near-field condition is met in our case of an air gun with h/λ of nearly 1/20. To investigate the dependence of the nongeometric

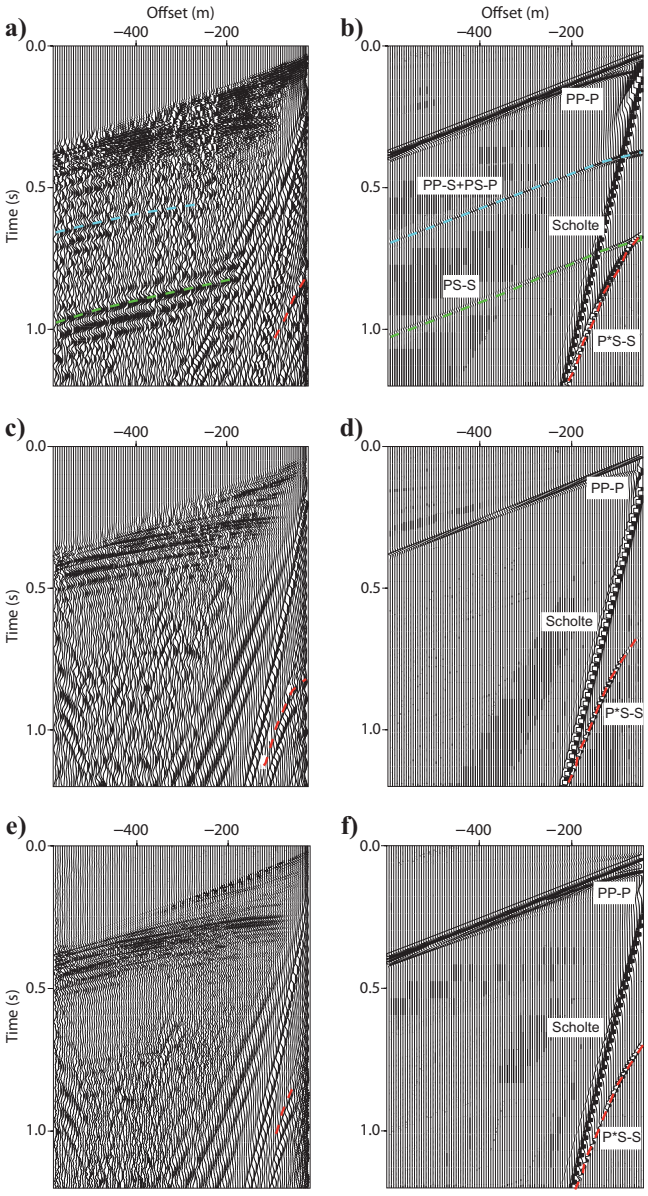

Figure 6. Comparison between field and synthetic data. Radial component of the (a) field data and (b) synthetic data. Vertical component of the (c) field data and (d) synthetic data. Pressure component of the (e) field data and (f) synthetic data. The seismic arrivals are identified and labeled on the synthetic data.

shear-wave P*S amplitude on the distance of the source from the water bottom, we have modeled the transmission response for different h/λ ratios. To facilitate the comparison between the different transmission responses, we have used the same input wavelet with a dominant frequency of 100 Hz and have varied h/λ by changing only the source height with respect to the fluid/solid interface. The results are shown in Figure 9 for two receiver positions at a horizontal offset of 5 and 50 m and at 20 m depth below the interface. At the near-offset receiver position, the geometric and nongeometric PS-waves interfere, and their amplitude is significant in the horizontal component when the ratio is at least 1:4 (Figure 9a and b). The vertical component becomes more important at larger offsets but only if the wavelength is eight times larger than the source height (Figure 9c and d). In the data set presented, the nongeometric PS-waves were very visible in the vertical component, but they showed a horizontal particle motion in the selected near-offset traces. At far offsets, these waves were contaminated by interface waves.

An interesting property of these waves is that they appear to be originating at a point on the interface directly below the source. This point acts as a generator from which the waves propagate with the S-wave speed of the sediments. At small offsets, the nongeometric S-wave is invisible. However, as the distance from the source increases, the relatively fast PS-waves, because of their increasing travelpath through water, arrive separately from the P*S-waves. This phenomenon is illustrated further in Figure 10. Here, we have computed the transmission response at a vertically placed receiver array for $h/\lambda = 1/8$ and $h/\lambda = 2$. The receivers are located 50 m away from the source and at depths between 5 and 100 m. For $h/\lambda = 1/8$, the P*S-wave, dominant in the horizontal and vertical components, is slightly delayed compared to the PS-wave at the deepest receiver. This delay in traveltime grows with decreasing receiver depth.

Furthermore, we can notice from Figure 11 that the dominant frequency of the PS-wave is higher than that of the transmitted P-wave for $h/\lambda = 1/8$ and is similar to it for $h/\lambda = 2$. However, the dominant frequency of the nongeometric shear wave is smaller compared to the P-wave. This can be explained by the fact that a source wavelet is composed of a broad range of frequencies. The high frequencies are in the far-field when they approach the water-bottom contact, giving rise to the PS-wave; whereas the low frequencies interact in the near-field, generating two additional types of converted waves: the P*S-wave and the PS head wave (a wavefront propagating with the S-wave velocity in the solid and with the P-wave velocity along the water bottom; see Figure 8). For that, we can conclude that the interaction with the water bottom has a frequency filtering effect. Consequently, the arrival identified as a PS-wave on the synthetic data is in fact a superposition of a geometrically converted wave and a head wave.

In global seismology, nongeometric shear-wave arrivals have been studied in theory extensively (e.g., Hron and Mikhailenko,

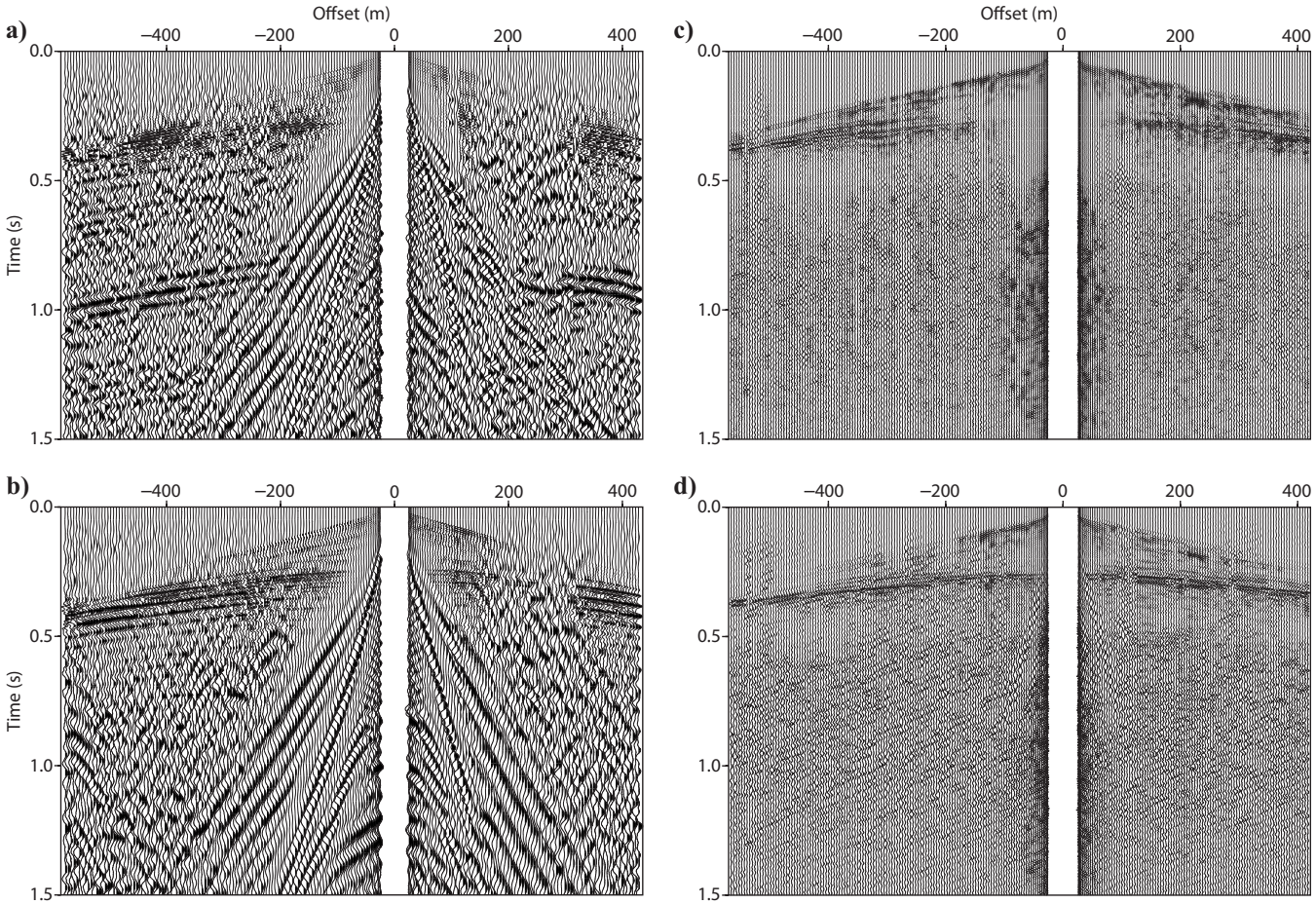

Figure 7. Comparison between common-receiver gathers recorded with an air-gun source and a water-gun source. (a) Horizontal and (b) vertical components of the air-gun data. (c) Horizontal and (d) vertical components of the water-gun data.

1980; Daley and Hron, 1983a, 1983b, 1988) but hardly observed in field data (Gutowski et al., 1984). These nongeometric events are interpreted to be the result of interaction of inhomogeneous waves with a plane interface (Hron and Mikhailenko, 1981). The inhomogeneous waves with the real part of the horizontal slowness p lying in the range $1/V_P < p < 1/V_S$ are taken into account in the Sommerfeld integral representation of the spherical wavefront radiated by a point source (Aki and Richards, 2002).

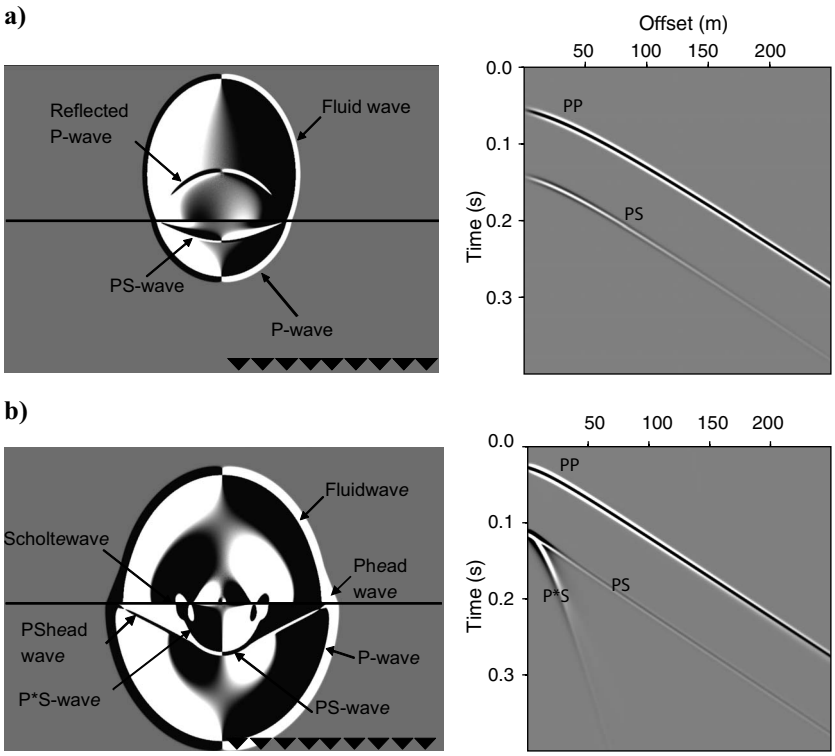

Figure 8. The horizontal particle velocity generated by a source in the fluid and computed for a fluid-solid configuration in (a) far-field ($\lambda \ll h$) and (b) near-field ($\lambda \gg h$) conditions. The response is computed for receivers buried in the solid, denoted by black triangles in the snapshot (left).

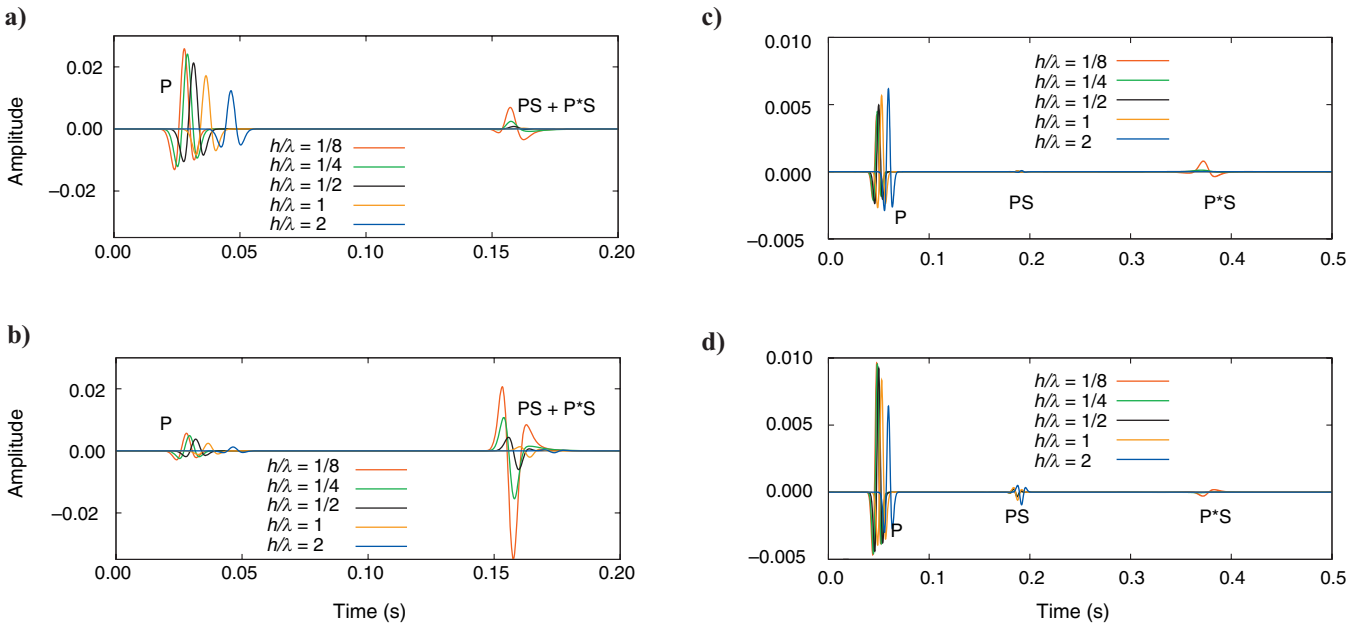

Figure 9. Excitability of the nongeometric S-wave for different h/λ ratios. The (a) horizontal and (b) vertical particle velocity recorded at a receiver located 5 m away from the source and 20 m below the water-bottom interface. The (c) horizontal and (d) vertical particle velocity recorded at a receiver located 50 m away from the source and 20 m below the water-bottom interface.

DISCUSSION

In the presented field data, two types of P-to-S-mode conversion have been identified: waves converted at the water bottom and waves converted at a reflector. The waves converted at a reflector are poorly visible and less continuous; large offsets appear to be more favorable to acquire these waves. However, the waves converted at the water bottom are clearly observable over a wide offset range. The interpretation of these two types of conversion is simplified by their low moveout velocity and linear horizontal particle motion.

The most interesting aspect of our field data is the observation of nongeometric PS-waves in the vertical and horizontal components as well as in the pressure component. These waves have been identified only in the low-frequency air-gun data, implying that this type of conversion occurs when the incident wavefield interacts with the water bottom in the near-field. We successfully verified the existence of these converted modes in a modeling study of the coupling effect between the source and water bottom for an elastic, isotropic, homogeneous half-space. Effects such as interaction of the source with the free surface, nonlinear deformation in the sediments, and attenuation on the excitation of P*S-waves still need to be studied.

The nongeometric waves behave as if they were generated by a shear source located on the water bottom. Therefore, they can be suitable for determining V_S in the sediments. In practice, acquiring this type of wave required placing a source with low frequency content close to the water bottom. This seems contradictory to what is common in shallow seismic surveys, where the focus is usually on the increase of resolution by including high frequencies. However, because of the effect of high V_P/V_S of the sediments on the wavelength, the resolution is not deteriorated when nongeometric converted waves are used. The resolution can even be better if V_P/V_S is very high, as in the case of shallow unconsolidated marine sediments.

The acquisition of the P*S-waves will be challenging for several reasons: (1) these waves are generated only when the wavelength is at least four times larger than the source height; (2) they have a narrow optimum offset window because they are observable at small offsets and are asymptotic to the strong interface waves; and (3) much denser spatial sampling is needed as a result of their low velocity. Hence, proper tuning of field parameters is essential to detect these waves.

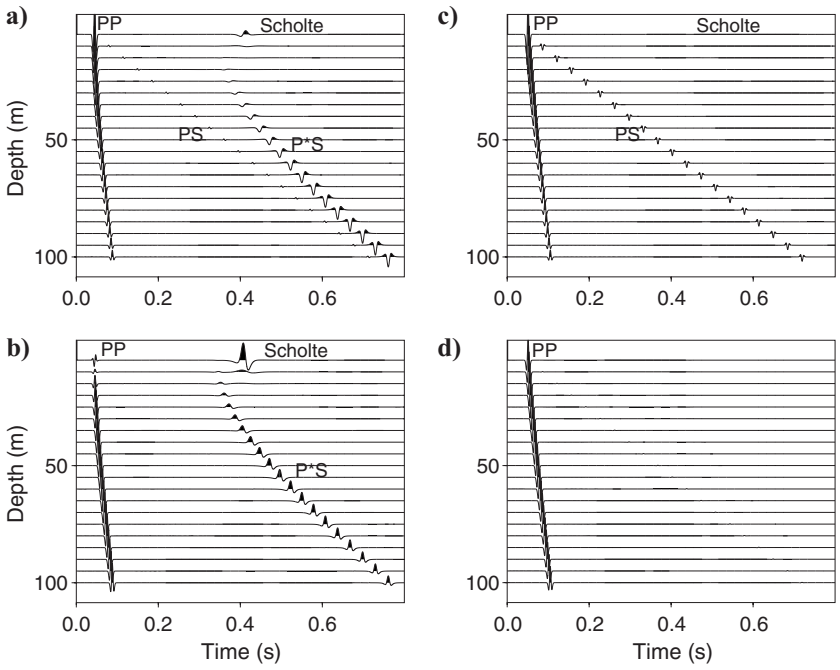

Figure 10. The particle velocity computed for two h/λ ratios. The receivers have an offset of 50 m and are located at depths between 5 and 100 m below the interface. Particle velocity for $h/\lambda = 1/8$ in (a) horizontal and (b) vertical directions. Particle velocity for $h/\lambda = 2$ in (c) horizontal and (d) vertical directions.

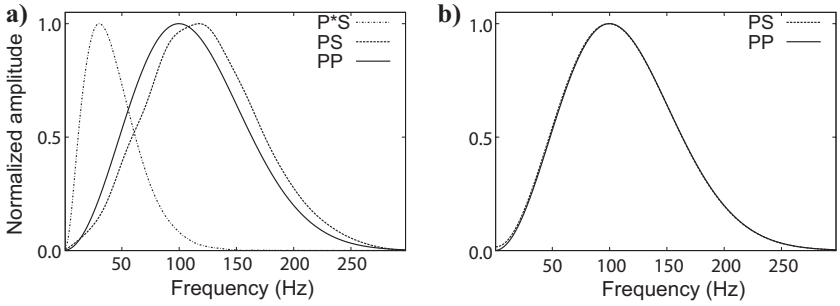

Figure 11. Frequency spectrum of the separate events shown in Figure 10. (a) Frequency spectrum of PP-, PS-, and P*S-waves recorded in the horizontal component at 50-m depth for $h/\lambda = 1/8$. (b) Frequency spectrum of PP- and PS-waves recorded in the horizontal component at 50 m depth for $h/\lambda = 2$. The amplitude of the frequency spectrum is normalized.

CONCLUSIONS

The data set presented in this study demonstrates the feasibility of acquiring P-to-S-converted waves in a shallow marine environment characterized by a high V_P/V_S ratio. The specific field setting at our survey area provided new insights on how to improve the poor P-to-S-wave conversion at the water bottom and helped us discover a new nongeometric S-wave arrival.

By comparing field data with modeling results, we have shown the presence of waves converted at the water bottom as well as at a subsurface reflector. The large delays in traveltimes and the linear horizontal motion associated with these waves simplify their interpretation in field data.

Furthermore, we discovered that nongeometric shear waves are excited when the dominant wavelength of the source is much larger than the source height with respect to the water bottom. The amplitude of these waves decreases as the distance between source and water bottom is increased. Kinematically, the waves behave as if they are excited by a shear source located at the water bottom. This specific type of converted wave can be useful for determination of V_S profiles in shallow marine sediments.

ACKNOWLEDGMENTS

The authors are grateful to the reviewers for improving the paper. This work is supported by The Netherlands Research Centre for Integrated Solid Earth Science (ISES).

APPENDIX A

KINEMATICS OF GEOMETRIC AND NONGEOMETRIC PS-S-WAVE REFLECTIONS

The geometric PS-S-wave reflection is converted at the water bottom according to Snell's law and is therefore explained by the classical ray theory. However, the nongeometric P-SS-wave travels only in the vertical direction as an evanescent wave before being converted to a propagating mode at the water-bottom interface. Therefore, they appear to originate at the projection point of the source on this interface. In this appendix, we demonstrate the difference in the kinematic behavior of the geometric and nongeometric P-SS-waves by deriving their traveltime expressions. Figure A-1 displays the travelpaths of the reflections and the geometric variables used for the derivation. Furthermore, we show that the geometric P-SS is interfering with two refracted modes in the offset range discussed in this article.

The traveltime t_{PSS} for the geometric converted mode PS-S as a function of offset x is

$$t_{PSS} = \frac{\sqrt{x_1^2 + z_1^2}}{\alpha_1} + \frac{\sqrt{(x - x_1)^2 + 4z_2^2}}{\beta_2}. \quad \text{(A-1)}$$

The conversion point x_1 can be determined by rewriting Snell's law in terms of the geometric variables defined in Figure A-1:

$$\frac{\sin\theta_1}{\alpha_1} = \frac{\sin\theta_2}{\beta_2},$$

$$\frac{x_1}{\alpha_1\sqrt{x_1^2 + z_1^2}} = \frac{x - x_1}{\beta_2\sqrt{(x - x_1)^2 + 4z_2^2}}. \quad \text{(A-2)}$$

To solve for x_1, equation A-2 is rearranged into the quartic equation of the form

$$x_1^4 + ax_1^3 + bx_1^2 + cx_1 + d = 0, \quad \text{(A-3)}$$

where

$$a = \frac{2x(\alpha_1^2 - \beta_2^2)}{\beta_2^2 - \alpha_1^2},$$

$$b = \frac{\beta_1^2(x^2 + 4z_2^2) - \alpha_1^2(z_1^2 + x^2)}{\beta_2^2 - \alpha_1^2},$$

$$c = \frac{2\alpha_1^2 z_1^2 x}{\beta_2^2 - \alpha_1^2},$$

$$d = \frac{\alpha_1^2 z_1^2 x^2}{\beta_2^2 - \alpha_1^2}. \quad \text{(A-4)}$$

Four possible solutions to this fourth-order polynomial exist: two real and two complex. The general form of these solutions is given in

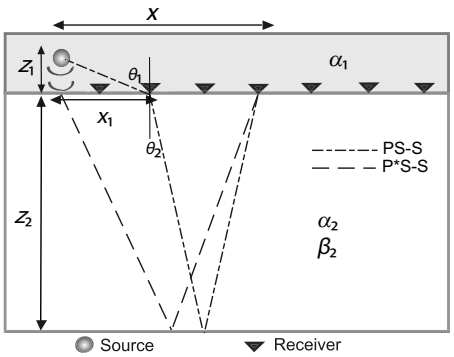

Figure A-1. Sketch of PS-S and P*S-S travelpaths. Definitions of the geometric variables used in the equations are also included.

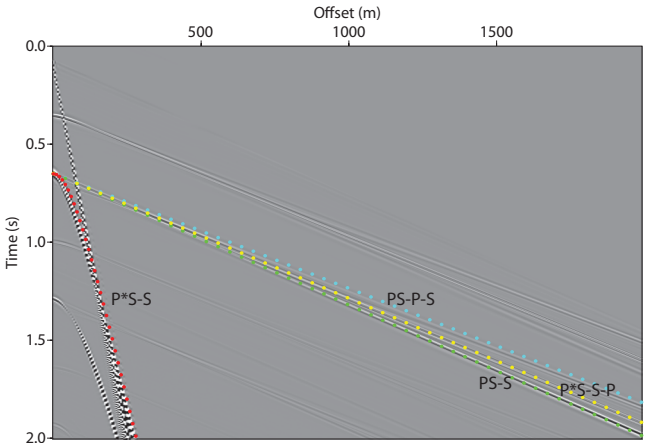

Figure A-2. The synthetic response is overlain by the traveltime curves of the reflected PS-S (green) and P*S-S (red) modes and the refracted PS-P-S (blue) and P*S-S-P (yellow) modes. The direct arrival is muted.

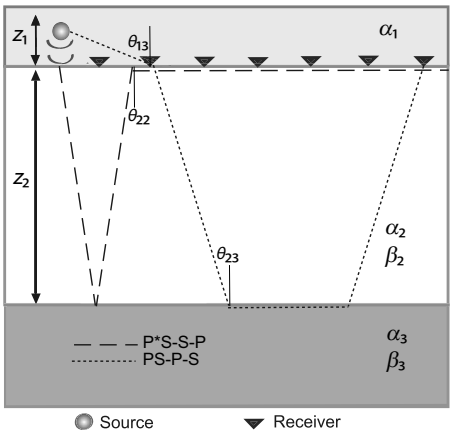

Figure A-3. Sketch of PS-S and P*S-S travelpaths. Definitions of the geometric variables used in the equations are also included.

detail by Taylor (1989). The exact solution for x_1 is the real number ranging between zero and x. This number can in turn be substituted into equation A-1 to compute the traveltime of the PS-S mode.

The P*S-S-wave appears to be originating at the fluid/solid interface, from where it propagates as a pure S-wave. Therefore, the traveltime of this arrival is

$$t_{\mathrm{P^*SS}} \approx \frac{\sqrt{(x^2 + 4z_2^2)}}{\beta_2}. \tag{A-5}$$

We computed the traveltimes of the two PS-S reflections for the model parameters used in the modeling study and compared these to the horizontal component of the synthetic data in Figure A-2. The difference in moveout between PS-S- and P*S-S-waves is caused by the conversion at the water bottom. For the PS-S-wave, the moveout is determined by the sound speed in water and the shear-wave velocity in the sediments given by the two terms in equation A-1. However, the moveout of the P*SS-wave is solely determined by the shear-wave velocity, resulting in a very low apparent velocity.

In Figure A-2, one can also notice that the PS-S-wave arrival is interfering with two other events at the offset range ($\sim$500 m) discussed in this article. These two events appear to be refractions traveling along the paths indicated in Figure A-3. For completeness, we also derived their traveltime expressions.

The traveltime of the refraction propagating as a P-wave along the boundary separating the two sediment layers is given by

$$t_{\mathrm{PSPS}} = \frac{x}{\alpha_3} + \frac{z_1 \cos\theta_{13}}{\alpha_1} + \frac{2z_2 \cos\theta_{23}}{\beta_2}, \tag{A-6}$$

where

$$\theta_{13} = \sin^{-1}\frac{\alpha_1}{\alpha_3},$$

$$\theta_{23} = \sin^{-1}\frac{\beta_2}{\alpha_3}. \tag{A-7}$$

The nongeometric P*S-S-wave is also refracted at the water-bottom interface. The traveltime of this refraction can be expressed by

$$t_{\mathrm{P^*SSP}} = \frac{x}{\alpha_2} + \frac{2z_2 \cos\theta_{22}}{\beta_2}, \tag{A-8}$$

where

$$\theta_{22} = \sin^{-1}\frac{\beta_2}{\alpha_2}. \tag{A-9}$$

The traveltime curves of the refracted waves are also included in Figure A-2. These arrivals are visible in the synthetic data; however, the PS-S reflection is considered more significant because only one mode of conversion is involved.

REFERENCES

Aki, K., and P. G. Richards, 2002, Quantitative seismology, 2nd ed.: University Science Books.

Allouche, N., G. G. Drijkoningen, W. Versteeg, and D. G. Simons, 2008, Studying converted waves in shallow marine environment: Proceedings of the 9th European Conference on Underwater Acoustics (ECUA), 369–374.

Ayres, A., and F. Theilen, 1999, Relationship between P- and S-wave velocities and geological properties of near-surface sediments of the continental slope of the Barents Sea: Geophysical Prospecting, **47**, 431–441, doi: 10.1046/j.1365-2478.1999.00129.x.

Caiti, A., T. Akal, and R. Stoll, 1994, Estimation of shear wave velocity in shallow marine sediments: IEEE Journal of Oceanic Engineering, **19**, no. 1, 58–72, doi: 10.1109/48.289451.

Chmela, B., 2003, Innovative non-conventional techniques for focused reservoir imaging: First Break, **21**, 44–46.

Daley, P. F., and F. Hron, 1983a, High frequency approximation to the nongeometrical S* arrival: Bulletin of the Seismological Society of America, **73**, 109–123.

———, 1983b, Nongeometric arrivals due to highly concentrated sources adjacent to plane interfaces: Bulletin of the Seismological Society of America, **73**, 1655–1671.

———, 1988, A non-geometrical SH-arrival: Geophysical Prospecting, **36**, 430–445, doi: 10.1111/j.1365-2478.1988.tb02172.x.

Domenico, S. N., 1984, Rock lithology and porosity determination from shear and compressional wave velocity: Geophysics, **49**, 1188–1195, doi: 10.1190/1.1441748.

Ewing, J., J. A. Carter, G. H. Sutton, and N. Barstow, 1992, Shallow water sediment properties derived from high-frequency shear and interface waves: Journal of Geophysical Research, **97**, no. B4, 4739–4762, doi: 10.1029/92JB00180.

Gehrmann, T., P. Gimpel, and F. Theilen, 1984, Marine shear wave profiling: 54th Annual International Meeting, SEG, Expanded Abstracts, 592–594.

Granli, J. R., B. Arntsen, A. Sollid, and E. Hilde, 1999, Imaging through gas-filled sediments using marine shear-wave data: Geophysics, **64**, 668–677, doi: 10.1190/1.1444576.

Gregory, A. R., 1976, Fluid saturation effects on dynamic elastic properties of sedimentary rocks: Geophysics, **41**, 895–921, doi: 10.1190/1.1440671.

Gutowski, P. R., F. Hron, D. E. Wagner, and S. Treitel, 1984, S*: Bulletin of the Seismological Society of America, **74**, 61–78.

Hamilton, E. L., 1976, Shear-wave velocity versus depth in marine sediments: Reviews of Geophysics, **41**, 985–996, doi: 10.1190/1.1440676.

———, 1979, V_P/V_S and Poisson's ratios in marine sediments and rocks: Journal of the Acoustical Society of America, **66**, 1093–1101.

Hron, F., and B. G. Mikhailenko, 1980, Discovery of a new nongeometrical S* arrival generated at a free interface: Proceedings of the 17th Assembly of the European Seismological Commission, 293–297.

———, 1981, Numerical modeling of nongeometrical effects by the Alekseev-Mikhailenko method: Bulletin of the Seismological Society of America, **71**, 1011–1029.

Kugler, S., T. Bohlen, T. Forbriger, S. Bussat, and G. Klein, 2007, Scholte-wave tomography for shallow-water marine sediments: Geophysical Journal International, **168**, 551–570, doi: 10.1111/j.1365-246X.2006.03233.x.

Park, C. B., R. D. Miller, J. Xia, J. Ivanov, G. V. Sonnichsen, J. A. Hunter, R. L. Good, R. A. Burns, and H. Christian, 2005, Underwater MASW to evaluate stiffness of water-bottom sediments: The Leading Edge, **24**, 724–728, doi: 10.1190/1.1993267.

Riedel, M., and F. Theilen, 2001, AVO investigations of shallow marine sediments: Geophysical Prospecting, **49**, no. 2, 198–212, doi: 10.1046/j.1365-2478.2001.00246.x.

Ritzwoller, M. H., and A. L. Levshin, 2002, Estimating shallow shear wave velocities with marine multicomponent seismic data: Geophysics, **67**, 1991–2004, doi: 10.1190/1.1527099.

Schmidt, H., 1988, SAFARI user's guide: SACLANT Undersea Research Centre, http://acoustics.mit.edu/faculty/henrik/oases.html, accessed 29 September 2010.
Schmidt, H., and G. Tango, 1986, Efficient global matrix approach to the computation of synthetic seismograms: Geophysical Journal of the Royal Astronomical Society, **84**, 57–67.
Stewart, R. R., J. E. Gaiser, R. J. Brown, and D. C. Lawton, 2003, Converted-wave seismic exploration: Applications: Geophysics, **68**, 40–57, doi: 10.1190/1.1543193.
Taylor, G. G., 1989, The point of P-S mode converted reflection: An exact determination: Geophysics, **54**, 1060–1063, doi: 10.1190/1.1442734.
Theilen, F. R., and I. A. Pecher, 1991, Assessment of shear strength of the sea bottom from shear wave velocity measurements on box cores and in-situ: Shear waves in marine sediments, *in* J. M. Hoven, M. D. Richardson, and R. D. Stoll, eds., Shear waves in marine sediments: Kluwer Academic Publishers, 67–74.
Westerdahl, H., P. Sparrevik, C. Madshus, L. Amundsen, and J. P. Fjellanger, 2004, Development and testing of a prototype seabed coupled shear wave vibrator: 74th Annual International Meeting, SEG, Expanded Abstracts, 929–932.